Research Square

Preprints are preliminary reports that have not undergone peer review.
They should not be considered conclusive, used to inform clinical practice,
or referenced by the media as validated information.

How Uncertain Are Estimates of Marine Carbon Dioxide Removal? Insights from a Simplified Model

Ruth Musgrave

rmusgrave@dal.ca

Dalhousie University

Article

Keywords:

Posted Date: June 25th, 2026

DOI: https://doi.org/10.21203/rs.3.rs-10006849/v1

License: This work is licensed under a Creative Commons Attribution 4.0 International License.
Read Full License

Additional Declarations: No competing interests reported.

How Uncertain Are Estimates of Marine Carbon Dioxide Removal? Insights from a Simplified Model

Ruth Musgrave

Department of Oceanography, Dalhousie University, Canada

rmusgrave@dal.ca

ABSTRACT

Marine carbon dioxide removal (mCDR) approaches such as Ocean Alkalinity Enhancement (OAE) and Direct Ocean Removal (DOR) are necessarily evaluated using ocean models, yet uncertainties in model predictions remain poorly understood. Here, we use a one-dimensional ocean model to investigate the controls on uncertainty in atmospheric CO_2 drawdown in an abiotic system. We show that, within the first few years after deployment, estimates of carbon removal are highly sensitive to mixed-layer physical and biogeochemical properties, while longer-term uncertainties are dominated by vertical mixing, air–sea gas exchange and the depth of the initial deployment. Using a Monte Carlo framework, we demonstrate that uncertainty in carbon drawdown can persist for decades when transport into the ocean interior occurs on timescales comparable to or faster than air–sea equilibration. These results identify a fundamental challenge for regional and global mCDR simulations, where the governing physical processes are often poorly constrained and subject to substantial spatial and temporal biases. Critically, uncertainty in the time evolution of carbon removal leads directly to uncertainty in the timing of net neutrality, with important consequences for monitoring, verification, and carbon crediting frameworks.

1 Introduction

The sequestration of atmospheric carbon dioxide in the ocean has received increasing attention over the past few years, with a series of National Academies of Science reports urging research into the risks, benefits and scalability of Carbon Dioxide Removal (CDR) in order to meet the warming threshold of 2°C prescribed by the Paris Agreement [1, 2, 3]. Emission cuts remain vital, however it is increasingly recognized that legacy CO_2 will remain in the atmosphere for many years, leading to ongoing warming unless actions are taken to remove it. Two marine Carbon Dioxide Removal (mCDR) techniques under consideration are Ocean Alkalinity Enhancement (OAE) or Direct Ocean Removal (DOR), both of which rely on reducing the partial pressure of carbon dioxide in the surface ocean leading to the drawdown of atmospheric CO_2 into the ocean [4, 5].

The atmospheric carbon dioxide removed by a given intervention increases in time as the water comes into equilibrium with the atmosphere via the process of air-sea gas exchange. At equilibrium, the theoretical maximum CDR has been achieved, with stoichiometric calculations for OAE of around 0.8 mol of CO_2 per mol of added alkalinity [5]. However, it can take years to decades for full equilibration, with the time-evolution of CDR depending sensitively on the rate of loss of an OAE or DOR intervention from the mixed layer compared to the rate of air-sea gas exchange [6, 7].

Given the difficulties associated with direct measurements of carbon dioxide drawdown over the large space and time scales associated with air-sea gas exchange, the use of ocean models for quantifying carbon drawdown associated with a given intervention seem unavoidable [8, 9]. However, understanding the sensitivities of CDR calculations to uncertainties in the ocean state is hindered by the complexity of the models that we use. Ocean models comprise coupled fluid dynamical, geochemical and biological components that represent the myriad complex processes that determine the ocean state. While some aspects are modelled directly from first principles, many components are necessarily parameterized due to computational expense (e.g. turbulent mixing) or complexity (e.g. biology). Still other aspects are simply not modelled at all, with the underlying assumption that such processes do not affect the ocean state at scale.

To date, uncertainties in CDR estimates have been derived from the intrinsic variability of global models [e.g. 10, 11], but such models often employ fixed parameterizations that, in effect, reduce the variability of a given parameter in the model compared to observations. For example, vertical mixing is often represented as a spatially and temporally constant eddy diffusivity, or the air-sea gas transfer coefficient is parameterized based only on wind speed. Bulk parameters in such models are tuned to best match large scale circulation patterns, such as the overturning circulation, with uncertain impacts on the advective and diffusive pathways of CDR tracers that are necessarily regionally localized. Accurately simulating tracers is non-trivial, as they are sensitive to both numerical methods and unresolved physical processes [12, 13], resulting in tracer pathways that are highly sensitive to model parameters. This study employs an abiotic reduced-complexity 1D model that

enables a systematic examination of how uncertainties in the simulated ocean state affect the calculation. This model does not fully represent ocean dynamics, perhaps most importantly ignoring advective processes that can lead to subduction, outcropping and shear dispersion. However, it enables a rapid exploration of parameter space and a mechanistic understanding of vertical processes that can be used to better inform our understanding of sensitivities in realistic models, and can be used to prioritize validation metrics. Using a Monte Carlo approach and running over 1000 simulations, the distributions of CDR estimates as a function of time across an ensemble of model runs are developed, demonstrating how combined uncertainties in physical processes and watermass properties (specified here using ranges of observed natural variability) manifest as uncertainties in the calculation of CDR. Uncertainties in the time-evolution of CDR due to a specific intervention have implications for both the award of carbon credits, and the time-scale over which a it becomes carbon negative after accounting for the Life Cycle Analysis (LCA) carbon costs of producing and distributing the addition [e.g. 14]. As such, these results have implications for the Monitoring, Recording and Verification (MRV) of carbon drawdown due to OAE and DOR using ocean models, which relies on well quantified uncertainties.

2 Results

The 1D diffusion model evolves Total Alkalinity (TA) and Dissolved Inorganic Carbon (DIC), allowing for the air-sea gas exchange of CO_2 to determine the flux of DIC at the surface (see Methods section for details). Here it is used to investigate the sensitivities in calculations of Carbon Dioxide Removal (CDR) due to an alkalinity enhancement intervention when modeled turbulent diffusion, air-sea gas exchange, and watermass properties are uncertain. CDR is calculated from pairs of model simulations, comprising both a baseline (control) and OAE/DOR (intervention) run. The Carbon Dioxide Removal (CDR) is defined as the difference in carbon uptake between the pair:

$$CDR = U_i - U_b \tag{1}$$

where U_i and U_b are the intervention and baseline uptakes, respectively. Sensitivities are then assessed by comparing *Sensitivity simulations* (with perturbed model parameters) to a *Reference simulation* (with mean model parameters). Changes in CDR between the sensitivity and reference simulation are captured in the CDR sensitivity ratio:

$$r_{CDR}(t) = \frac{CDR_{sen}(t)}{CDR_{ref}(t)}. \tag{2}$$

2.1 Sensitivities of CDR estimates to biases in the modelled ocean state

Perturbing individual model parameters by values consistent with observed variability (see Table 1) leads to CDR estimates that vary by up to a factor of two within the first few years after deployment of the intervention, dropping to differences of between 10-20% between 20-50 years (Figure 1). CDR estimates are sensitive to different parameter uncertainties at different times following the intervention, in contrast to the uncertainties associated with the individual base and intervention simulations that contribute to the CDR estimate for whom uncertainties accumulate in time. This fundamental difference in behaviour can be attributed to the fact that in the CDR case, the end state – where the full water column is in equilibrium with the atmosphere – will be very similar for all model parameters as it is the theoretical maximum drawdown for a given intervention.

The largest sensitivities tend to occur for most parameters within the first few years following an intervention, with changes that result in differences in the initial rate of air-sea gas exchange leading to the largest differences from the reference simulation. Air-sea gas exchange is determined by the initial DIC, TA, mixed layer depth, wind speed, gas transfer coefficient and deployment depth (Figure 1 b). Positive and negative perturbations of the background DIC and TA lead to CDR calculations that are almost double and half that of the baseline at the start of the simulation (Figure 1 b, red and black lines), while wind speeds, gas transfer coefficients and mixed layer depths contribute about 50% uncertainty. However, uncertainties arising from these parameters diminish in time, while those associated with pycnocline diffusivity (κ_{pyc}), wind speed and the gas transfer coefficient (cyan dashed lines, cyan solid lines, green dashed lines, magenta dashed lines) become increasingly important. These parameters relate to the interplay between uptake of atmospheric CO_2 compared to the rate at which TA and DIC are drawn down into the deep ocean. In particular, when pycnocline diffusivity is uncertain by an order of magnitude (a value that is within observed variability and model uncertainties; [15, 16]), uncertainties in CDR peak to up to 30% 2-3 years after the OAE addition. By the end of the simulation, the largest sensitivities in the CDR calculation come from deployment depth, pycnocline diffusivity, wind speed, the gas transfer coefficient and temperature.

Broadly speaking, sensitivites in the calculation can be considered to arise through three main processes. The first relates to changes in carbonate system buffering associated with changes in background alkalinity, DIC, temperature and salinity. These effects are most important for determining the change in surface pCO_2 associated with an intervention (and thus air-sea gas exchange) and for determining the theoretical maximum CDR for a given alkalinity addition [5]. The former of these processes is significant at early times, but overall this sensitivity at long times is limited by the range of variability in the theoretical

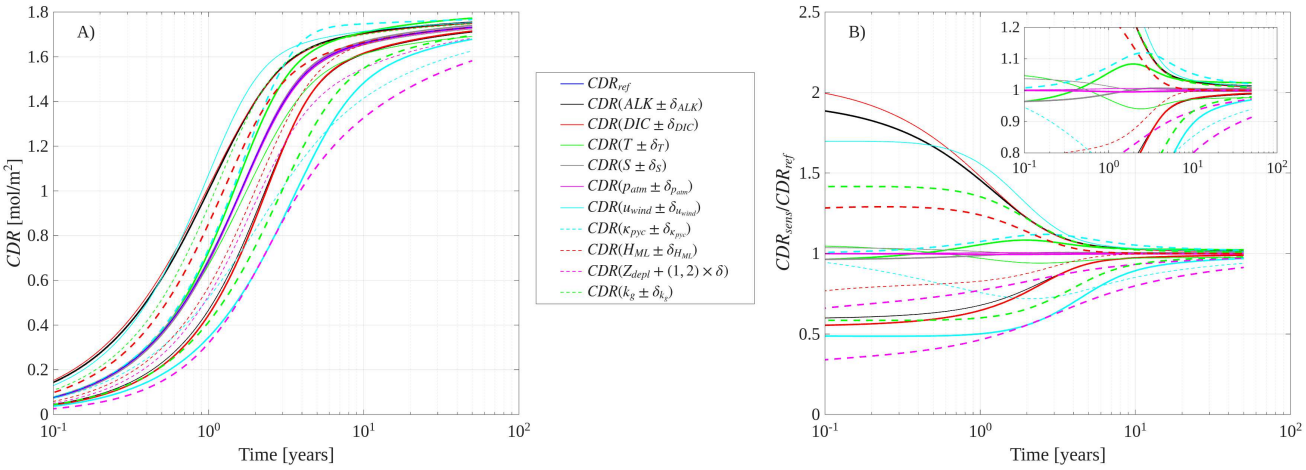


Figure 1. (A) CDR sensitivities due to OAE intervention in a 2000m deep ocean. Thin solid blue line is the Reference simulation, colours are Sensitivity simulations. Thin lines are positive perturbations to the background parameter, and thick lines are negative perturbations. (B) is as (A), but with the CDR curve of each sensitivity simulation normalized by that of the Reference simulation. Inset is as for (B) but zoomed in to better show sensitivities at late times. Note the logarithmic time axis to better distinguish the curves.

maximum efficiency in the global ocean, which amounts to only a few percent. The second set of sensitivities arise from the physical exchange of CO_2 with the atmosphere, and the downward transport of unequilibrated alkalinity into the deep ocean by turbulent mixing. Finally, CDR is strongly negatively affected by the deployment of alkalinity within or below the pycnocline, as illustrated by the sensitivity to the parameter Z_{depl}. This emphasizes the importance of outfall considerations to ensure that alkalinity is deployed in a manner that it is initialized in the surface ocean.

The sensitivity of CDR estimates to interior mixing and air-sea flux can be understood in terms of the relative timescales associated with these processes. For a box at the surface of the ocean that experiences no vertical mixing with the ocean below, the equilibration of CO_2 in the box follows an exponential function with the timescale for exchange given by

$$\tau_{air-sea} = \frac{H_{ML} I}{k_g R}. \tag{3}$$

where I is the ionization ratio, and R is the Revelle buffer factor [17]. This expression assumes linearized carbonate chemistry and has been widely used in the literature [e.g. 18]. In the interior, the timescale for alkalinity to mix into the deep ocean can approximately be represented by an exponential in time, with the timescale given by

$$\tau_{mix} = \frac{H_{ML} h_p (D - H_{ML})}{D \kappa_{pyc}} \tag{4}$$

where D is the ocean depth, and h_p is the thickness of the pycnocline (see Appendix C for a derivation).

With these timescales in mind, three characteristic temporal regimes can be defined.

1. Initial rapid-equilibration ($t \ll \tau_{mix}$): At early times before alkalinity is lost from the mixed layer, the uptake in each of the CDR pair simulations roughly follows an exponential with a timescale given by $\tau_{air-sea}$ (eq. 3). Estimates of CDR during this period are sensitive to uncertainties in the parameters that determine this timescale, i.e. R, I, H_{ML} and k_g, as they lead to differences in this timescale between the reference and sensitivity simulations that manifests as large changes in the initial uptake.

2. Alkalinity loss from the mixed layer ($t \approx \tau_{mix}$): At this time, vertical mixing has removed a significant fraction of the alkalinity from the surface layer into the lower layer. As the initial air-sea equilibration is roughly exponential in time, the fraction of alkalinity that has equilibrated with the atmosphere roughly follows $\exp(-\tau_{mix}/\tau_{air-sea})$, with higher CDR efficiencies having been achieved for larger values of the argument. Estimates of CDR at this time are predicted to be sensitive to all of the parameters appearing in equations 4 and 3, however for the simulations presented here, the largest

CDR sensitivities are associated with κ and k_g as the uncertainties on these values have the largest magnitude.

3. Deep mixing ($t \gg \tau_{mix}$): For large times, alkalinity becomes mixed throughout the depth of the ocean. A vertical gradient in DIC arises through equilibration of the upper ocean with the atmosphere, but it is gradually reduced by mixing, which also brings deep, unequilibrated alkalized waters back up to the surface where it equilibrates. It is this slow process of equilibration of the deep, unequilibrated waters that leads to parameter sensitivities in CDR that exist for many decades, with magnitudes that are particularly significant for uncertainties in pycnocline diffusivity and the gas transfer coefficient.

Thus, uncertainty in pycnocline diffusivity impacts estimates of CDR in two ways: first, it determines the fraction of equilibrated alkalinity before it mixes into the deep ocean, and secondly it determines the rate at which the deep unequilibrated alkalinity mixes back into the surface layer. As such it plays a role in both the magnitude and longevity of CDR uncertainties.

2.2 Combining uncertainties

To assess how simultaneous model biases could combine to produce a final uncertainty in the estimated CDR, a Monte Carlo approach is employed. The simulations demonstrate that – as for the sensitivity simulations of the previous section – uncertainties in CDR estimates are maximal within the first few years after deployment during the initial rapid-equilibration phase, where sensitivities to both carbonate system and physical parameters affect the calculation. Uncertainties are determined from these ensembles by quantifying the spread of estimates at a given time post deployment (Fig 3). The distribution of CDR estimates by members of the ensemble after two years is almost uniform, with some estimates of the CDR being almost zero, while other ensemble members estimate values 50% greater than the reference simulation (Figure 3a). This behaviour is captured in ε_{20}, which shows that more than 80% of ensemble members estimate CDR that is more than 20% discrepant with the Reference simulation during this period (Figure 3 b). After this period, however, the uncertainties drop off rapidly, with ε_{20} decreasing from around 0.8 to 0.4 within five of years of deployment. Subsequently, the range of uncertainties narrows further at a slower rate, as the full water column comes into equilibrium with the atmosphere.

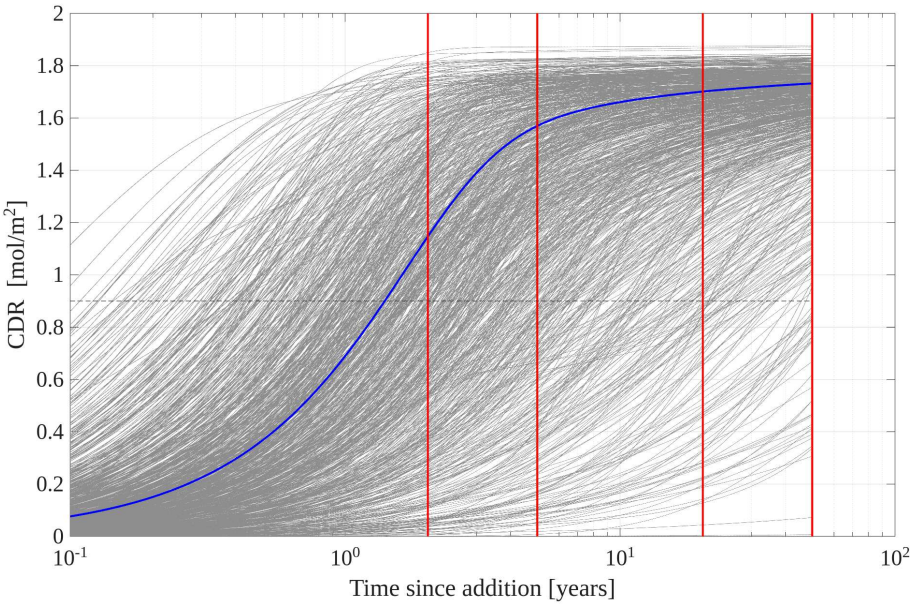


Figure 2. Monte Carlo ensemble CDR estimates over time in a 2000m deep ocean. Blue line is the CDR curve for the Reference simulation. Red lines indicate the times used to construct the uncertainty probability distribution functions in Figure 3. Black dashed line is at 50% total CDR, used to estimate the times to net neutrality in Section 4.

An identical ensemble simulation performed in a 200 m deep ocean exhibits similar behaviour (Figure 3 b). Uncertainty evolution in the first phase of equilibration where only mixed layer properties and the gas transfer coefficient determine carbon drawdown are identical. At later times, however, the shallower ensemble has markedly reduced uncertainties compared to the deeper ensemble, as for most parameter values the entire water column is able to come into equilibrium within the 50 year simulation duration.

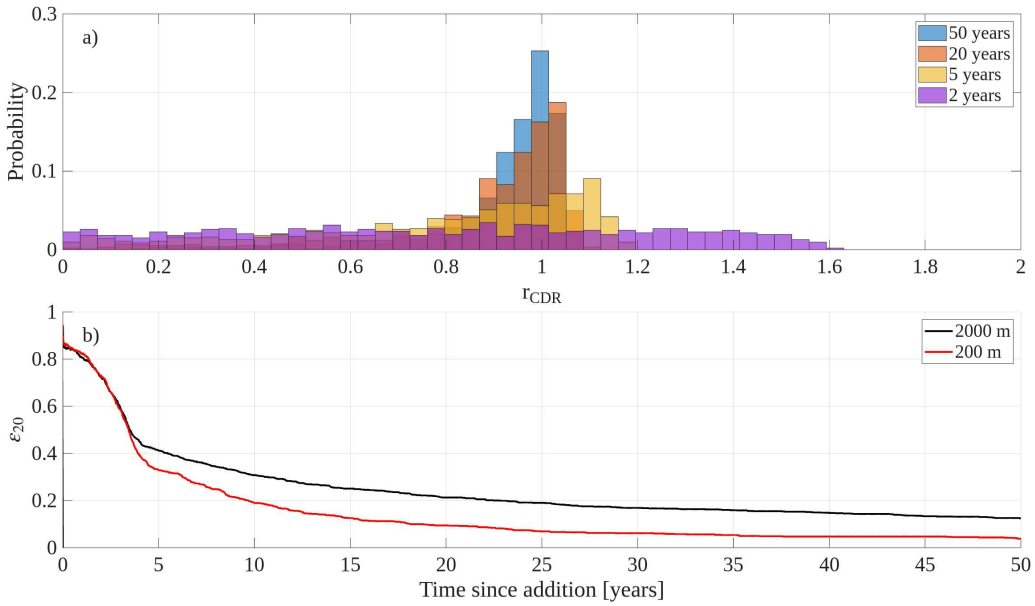


Figure 3. Monte Carlo uncertainties in CDR estimates over time. a) Probability distribution of the CDR associated with each ensemble member normalized by the Reference simulation (r_{CDR}) 2, 5, 20 and 50 years since deployment in a 2000m deep water column. b) Fraction of simulations with more than 20% difference in CDR compared to Reference simulation as a function of time for 2000 m deep (black line) and 200 m deep (red line) ensembles.

For deployments within the mixed layer, CDR estimates across the ensembles are strongly correlated with pycnocline diffusivity and wind speed, with higher estimates of CDR associated with ensemble members that have lower pycnocline diffusivities and higher wind speeds. The distribution of r_{CDR} as a function of $\exp(-\frac{\tau_{mix}}{\tau_{air-sea}})$, shown in Figure 4, demonstrates that when the mixing timescale is much longer than the air-sea gas exchange timescale, r_{CDR} converges to 1 rapidly and the water column comes into equilibrium relatively fast with low uncertainties at early times. However, when the mixing timescale is much shorter than the air-sea gas exchange timescale, r_{CDR} converges very slowly, maintaining large uncertainties for many decades after deployment. In the latter case, a significant fraction of the intervention is lost from the mixed layer at early times, and the timescale for those unequilibrated waters to resurface and equilibrate adds further sensitivities to interior mixing and air-sea gas exchange.

Finally, as for the sensitivity simulations, our Monte Carlo ensembles demonstrate the sensitivity of the overall efficiency of CDR on the deployment depth of the intervention (small dots, Figure 4). In all of these simulations, the initial deployment is no deeper than 100 m below the mixed layer, with most well within 50 m (see Fig 6), yet many of the CDR estimates associated with those deep deployments are significantly below the reference simulation even 50 years after deployment. Such deployments are both highly uncertain and highly inefficient.

3 Time to net neutrality

Though CDR estimates are expected to eventually converge on the theoretical maximum, the time taken to reach equilibrium can vary from a few years to many decades. This is particularly important when accounting for the Life Cycle Assessment (LCA) of a given CDR technology, as the equilibration time affects the time taken for a given intervention to become net carbon negative.

The time taken for a given deployment to become net carbon-negative depends on the time evolution of the CDR and the carbon cost of the deployment. [19] estimate that spreading 1.321 tCO_2 of $Ca(OH)_2$ in the ocean has the potential to uptake 1 t of CO_2, with a carbon penalty of 449 kg CO_{2eq}. Thus, for a nominal carbon cost of around 50% (or 0.8 mol/m^2 per 1.6 mol/m^2 of CO_2 removed), the parameters used in the reference simulations estimate a time to net-neutrality to be around 1.4 years (red line, Figure 5). However, the range of estimates of this time is large, with about 30% of the ensemble estimating the time to net neutrality to be under a year, and 50% of the ensemble estimating it to be longer than 2 years. Around 4% of the ensemble estimate the time to net neutrality to be longer than 50 years. The long tail in this distribution is associated with simulations wherein either the intervention was deployed below the mixed layer, or the intervention was mixed below the mixed layer before it could come into equilibrium with the atmosphere.

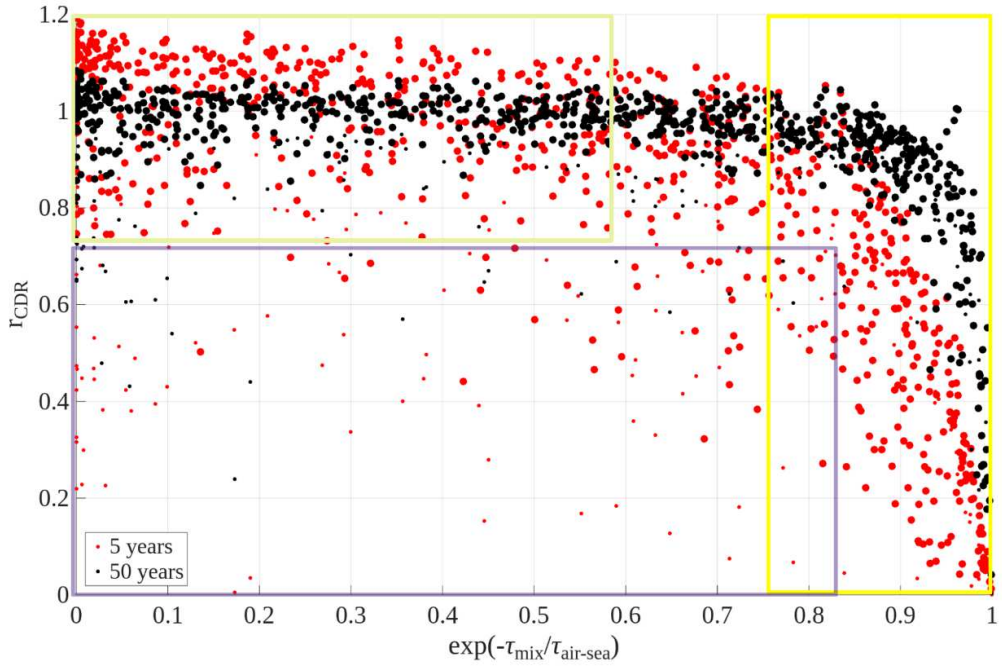


Figure 4. The distribution of CDR sensitivity ratio, r_{CDR}, after 5 and 50 years of integration is largely determined by the amount of equilibration that occurred during the rapid-equilibration phase. For members of the ensemble with low values of $\exp(-\tau_{mix}/\tau_{air-sea})$ (green box), r_{CDR} is close to one, indicating that all members of the ensemble have similar values and the water column is in equilibrium with the atmosphere. However, for members of the ensemble with high values of $\exp(-\tau_{mix}/\tau_{air-sea})$ (yellow box), r_{CDR} is poorly constrained, with a wide distribution of values that depend on specific model parameters. Small dots (purple box) indicate ensemble members where alkalinity was added below the mixed layer by no more than 100 m (see Fig 6).

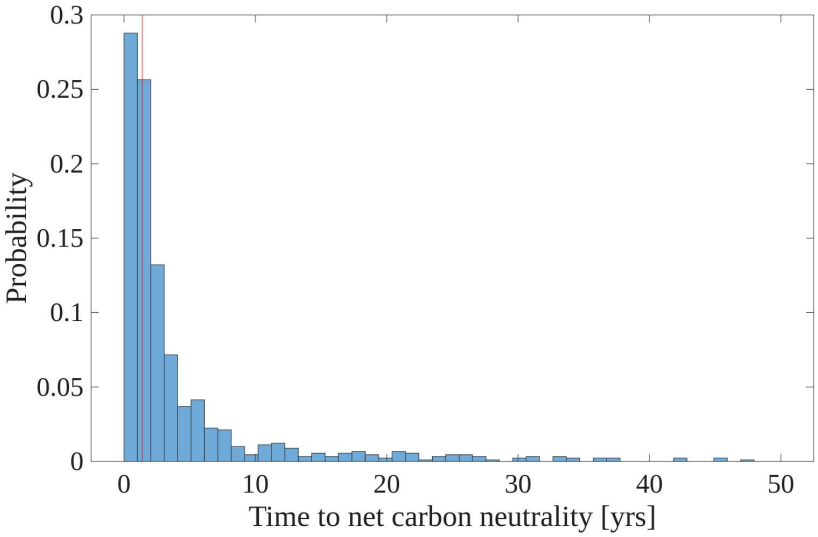


Figure 5. Distribution of estimates from the 2000 m deep Monte Carlo simulation of the time to net carbon neutrality assuming a 50% carbon cost (see black dashed line in Figure 2).

4 Discussion

The 1D model captures the interactions of vertical mixing, air-sea gas exchange and the carbonate system, elements that have already been demonstrated to be of central relevance to the uptake of carbon dioxide by mCDR interventions [7]. While uncertainties in the physical and biogeochemical water mass properties lead to large sensitivities in the first few years, uncertainties in interior diffusivity and the gas transfer coefficient can lead to uncertainties in CDR that can persist for decades, highlighting the importance of validating water mass properties, mixing and air-sea gas exchange in ocean models to be used for CDR. On the same timescales over which turbulent diffusion occurs, watermasses in the ocean advect, subduct and outcrop. These processes and their associated uncertainties are not represented here, but it is expected that they would contribute significant additional uncertainties over periods of years to decades, as the Lagrangian pathways traversed by fluid parcels are sensitive to model parameters such as resolution [20]. In particular, subduction will play an equivalent role to diffusivity, removing surface waters from contact with the atmosphere and contributing to uncertainties when air-sea equilibration timescales are long compared to subduction timescales.

In general, interior mixing and air-sea gas exchange are poorly constrained in ocean models. Both processes are predominantly determined by turbulence, which occurs in the ocean at scales of centimeters to meters. As such, the effects of turbulence are always parameterized and are subject to considerable uncertainty [21], with known sensitivities for global climate projections [e.g. 22, 23, 24]. Even with explicit mixing parameterizations, validating model mixing is challenging as some grid scale variance is removed by numerical truncation errors that are hard to quantify, and ocean measurements are hampered both by the intermittency that characterizes turbulent processes, and the specialized platforms that are required. As a result, it is difficult to know how accurately mixing is represented in a model using direct metrics. However, a comparison of estimates from the data assimilating state estimate ECCO product to observationally derived estimates demonstrated large (order of magnitude) differences in both the magnitude and vertical structure of turbulent diffusivities [16].

Gas transfer coefficients for air-sea gas exchange are similarly uncertain. The gas transfer coefficient sets the rate of atmosphere-ocean exchange for a given disequilibrium, and it fundamentally depends on the rate of renewal of the surface microlayer by near-surface turbulence [25] and the injection of bubbles by breaking waves [26]. The generation of such processes is highly complex, and as such, bulk parameterizations that depend only on wind speed, such as that used here and most commonly in ocean models, exhibit wide scatter and uncertainty in the exact value of gas transfer coefficient for a given wind speed [27]. Though regional biases arising from incomplete physics might broadly cancel out when considering global simulations, for CDR estimates in given locations, these biases can strongly affect the results leading to large uncertainties for a given intervention.

Finally, model representations of the carbonate system are known to be biased with respect to observational products, often arising as a result of weak physical exchange between the deep and surface ocean [28]. [29] demonstrate regional biases in alkalinity of 100 umol/kg between CMIP 5/6 simulations compared to the observationally derived GLODAPv2. The effects of such biases on OAE have been considered by [30], who estimates that initial pCO_2 reduction associated with OAE could be overestimated by up to 13%. These errors in the initial pCO_2 deficit due to an OAE intervention lead to the large uncertainties in the CDR estimate in the first few years shown in this work.

Without constraints, the combination of such global and regional model inaccuracies has the potential to lead to large uncertainties in CDR estimates made by the current generation of ocean models. In addition to those explicitly considered in the abiotic model presented here, further uncertainties may arise when considering the incomplete dissolution of an alkaline feedstock, wherein a fraction of what was added may sink to the seabed, or when considering the biological impacts of OAE that may alter alkalinity in the ocean.

This study is limited by the independent statistical representation of parameter uncertainties that, in reality, are coupled via underlying ocean dynamics. For example, high winds, which enhance air-sea gas exchange, also tend to generate cooler surface temperatures and large pycnocline diffusivities through shear-driven turbulence. The coupling of uncertainties deserves further exploration in future studies. Despite its limitations, the model has demonstrated that uncertainties in CDR calculations arising only from abiotic processes are significant, and warrants serious further investigation as this affects the quality of carbon credits that can be attributed to OAE or DOC interventions. Only by accounting for all such uncertainties can we ensure that interventions receiving carbon credits are genuinely carbon negative on timescales of years rather than decades.

5 Methods

Two tracers are considered: Dissolved Inorganic Carbon (DIC, $C = [CO_2^*] + [HCO_3^-] + [CO_3^{2-}]$ mol m^{-3}); and Total Alkalinity (A, mol m^{-3}). The tracers are assumed to obey the 1D diffusion equation:

$$\frac{\partial C}{\partial t} = \frac{\partial}{\partial z}\left(\kappa \frac{\partial C}{\partial z}\right)$$
$$\frac{\partial A}{\partial t} = \frac{\partial}{\partial z}\left(\kappa \frac{\partial A}{\partial z}\right) \tag{5}$$

with $\kappa(z)$ representing the turbulent diffusivity of the tracers. Flux boundary conditions are applied to ensure that a) there is no flux of alkalinity into or out of the domain; b) there is no flux of DIC out of the bottom of the domain, and c) the flux of DIC at the surface is determined by F_C, which arises from air-sea gas exchange of CO_2:

$$\left.\frac{\partial C}{\partial z}\right|_{z=-h} = 0 \qquad \left.\frac{\partial C}{\partial z}\right|_{z=0} = F_C$$
$$\left.\frac{\partial A}{\partial z}\right|_{z=-h} = 0 \qquad \left.\frac{\partial A}{\partial z}\right|_{z=0} = 0. \tag{6}$$

Air-sea flux is represented as

$$F_C = \frac{F_{pCO_2}}{\rho_0} = \frac{1}{\rho_0} k_g k_0 \Delta \mathrm{pCO_2} \tag{7}$$

where k_g is the gas transfer coefficient and k_0 is the solubility. Solubility is dependent on temperature and salinity, and is represented using the experimentally-derived parameters and expression in [31]. As is most commonly used in ocean models, the gas transfer coefficient is parameterized with a quadratic dependence on 10m wind speed,

$$k_g = 0.251 < U^2 > \left(\frac{Sc}{660}\right)^{-0.5} \tag{8}$$

[32, 33]. Sc is the temperature-dependent Schmidt number, defined as the kinematic viscosity of the water divided by the diffusion coefficient of the gas. For CO_2 it takes a value of 668 at 20°C.

With initial conditions and model parameters as described below, equations 5 are integrated forwards in time. F_C is re-calculated at each timestep using values of pCO_2 computed at the surface assuming equilibrium chemistry [34].

The carbon uptake in each simulation is calculated as the time integral of the air-sea flux:

$$U = \int^t F_C(C(0,t'),A(0,t'))\,dt'. \tag{9}$$

The numerical accuracy of the solution is confirmed by comparison to the depth integrated DIC, which, for the simulations presented in this paper is always within a few percent. The timestep is restricted so that the change in DIC during any given timestep does not result in a change in surface pCO_2 such that the sign of the air-sea flux changes. In practice this simply limits the magnitude of the initial disequilibrium between the atmosphere and ocean.

Initial conditions are prescribed for $C(z)$ and $A(z)$ with parameters as in Table 1 and functional forms described in Appendix A. Initial intervention profiles for $A(z)$ are defined by deployment depth (z_{depl}), which specifies the deepest depth of the deployment. Concentration profiles are uniform to the surface if the deployment depth is within the mixed layer, or within a layer of thickness 60 m if below the mixed layer. All intervention simulations have identical total alkalinity additions.

Model parameters such as mixed layer salinity (S_{ML}), mixed layer temperature (T_{ML}), atmospheric partial pressure (pCO_2), diffusivity (κ), gas transfer coefficient (k_g) and mixed layer depth (H_{ML}) vary between simulations but are fixed in time (in a more complex model they could be updated by physics or chemistry that is not simulated here). Deployment depth (z_{depl}) sets the initial condition of the intervention simulation, and this sensitivity attempts to capture the effects of near-field dosing processes, including particle dissolution dynamics, mixing and subduction. Such processes can result in some or all of the intervention being deployed beneath the surface layer (e.g. in the case of a subsurface outfall, negatively buoyant plume or the slow dissolution of negatively buoyant alkaline particles).

The following naming convention is used for the simulations:

- A *Baseline Simulation* is a single simulation performed without an OAE/DOR addition, from which U_b is computed.

- An *Intervention Simulation* is a single simulation performed with an intervention, from which U_i is computed. For this paper the intervention is always OAE, with an additional 2.048 mol/m^2 added as an initial condition (equivalent to a 100 μmol/kg change in concentration in a 20 m deep mixed layer). The underlying processes described here are identical for both OAE and DOR.

- The *Reference Simulations* are a pair of baseline and intervention simulations that use the reference model parameters, defined to be the values indicated in **mean** column of Table 1. CDR_{ref} is calculated from this pair.

- The *Sensitivity Simulations* are a series of pairs of baseline and intervention simulations that use the reference model parameters with positive or negative perturbations to a single parameter. Perturbations are chosen within the range of natural variability in the ocean at a given location. CDR_{sen} is calculated from this pair. Changes in CDR between the sensitivity and reference simulation pairs indicates the sensitivity of the CDR estimate to the model bias in the perturbed parameter.

A set of reference parameters are defined, along with statistical distributions that represent the uncertainty of that parameter in an ocean model. These distributions were chosen to represent the range of natural variability observed in the ocean at a given location. Uncertainties in atmospheric pressure, total alkalinity, dissolved inorganic carbon, temperature, salinity and wind speed are prescribed to be normally distributed, with means and standard deviations given in Table 1. Uncertainty in mixed layer depth and the logarithm of diffusivity is assumed to follow a Pearson Type 1 distribution, with non-zero kurtosis and skewness determining the asymmetry and tails of the distributions. The distribution of the gas transfer coefficient is derived from the combined uncertainties in wind speed, temperature and the gas transfer parameterization itself (see B). In general, the distributions have been chosen to approximately represent the variability in a given parameter at a fixed location, but additional justification for the distributions of the gas transfer coefficient and diffusivity are provided below.

The diffusivity in the interior of the model is determined by the profile of $\kappa(z)$, which represents the effects of turbulent mixing. Within the mixed layer it is fixed at 10^{-2} m^2/s for all simulations, but the deep diffusivity is varied, in doing so changing the diffusivity at the pycnocline (see Fig 7b). Diffusivity is not a prognostic variable in ocean models, and its prescription across different models is varied. In some, such as MOM6, diffusivity is parameterized using closures such as KPP at the surface [35], and tidal/internal wave mixing models in the interior [e.g. 36]. In others, such as ECCO, diffusivity is tuned to both maintain numerical stability and reproduce certain aspects of the model simulation. In still others, such as some versions of CESM, it is parameterized in the surface and set to a constant value in the interior. Studies that compare modeled and observed diffusivities are few and far between, but those that do exist show significant differences [e.g. 16]. Observed turbulent diffusivities range between 10^{-6}-10^{-2} m^2/s throughout the global ocean [15], with a canonical value for pycnocline diffusivity of 10^{-5} m^2/s [37, 38]. Diffusivities, as for other turbulent quantities, tend to be skew-log-normally distributed [39] and we assume such a distribution for deep diffusivities with a mean value of 10^{-5} m^2/s, and a standard deviation of one order of magnitude.

Observations indicate that the gas transfer coefficient varies throughout the global ocean with values between 0 - 150 cm/hr. Due to the convenience of measuring and inferring wind speed, the bulk parameterization (eq. 8) attributes a single value of gas transfer to a given wind speed [27], however, the parameters are derived from experiments that took place under diverse physical conditions, and as such there is a spread in the values that represent regional and temporal biases. The standard deviation in the gas transfer coefficient binned by wind speed increases with wind speed, with values of around 2 cm/hr at low wind speeds, and 24 cm/hr at high wind speeds (B). For simplicity, in this work we use a constant standard deviation of 4 cm/hr for all values of wind speed.

Finally, wind speed appears as a parameter in this model only through the parameterization for the gas transfer coefficient, k_g, though in reality one might expect wind speed to also affect the pycnocline diffusivity by increasing turbulent mixing in the upper ocean. The coupling between diffusivity and wind speed is complex and it is not represented here.

5.1 Sensitivity Simulations

To explore the sensitivity of the estimated CDR to each parameter in turn and determine a mechanistic understanding of the underlying processes, parameter perturbations are first considered in isolation. This results in 24 simulations corresponding to positive and negative perturbations of one standard deviation to the twelve parameters listed in Table 1. Deployment depth sensitivities are assessed differently, with the sensitivity simulations setting the deployment depth to 20 and 40 m below the mixed layer.

As the full water column comes into equilibrium, the CDR sensitivity ratio, r_{CDR}, will tend towards unity, however deviations from this equilibrium value are anticipated as properties such was water column temperature or background DIC alter the theoretical maximum CDR per unit alkalinity added, with typical values ranging between 0.8 and 0.95 [5]. This translates to a small percentage range of values for equilibrated r_{CDR} in these simulations.

5.2 Monte Carlo Simulations

The effects of simultaneous parameter uncertainties on the CDR calculation is explored using a Monte Carlo approach, wherein an ensemble of simulations comprising a baseline and intervention pair is run. Parameter biases across each pair are identical, and are selected at random from prescribed statistical distributions of each parameter and its uncertainty (Figure 6). Two ensembles are run with 200 and 2000 m deep domains to establish how uncertainties in the estimate of mCDR depend on ocean depth. Each ensemble has $N = 1000$ simulation pairs (baseline and intervention) that are integrated forwards in time for 50 years with 10 hour timesteps. To investigate the evolution of uncertainties in the Monte-Carlo simulations, we define the metric

$$\varepsilon_{20}(t) = \frac{1}{N}\sum_{i=1}^{N}(|r^i_{CDR}(t) - 1| < 0.2), \tag{10}$$

which captures the fraction of the ensemble within 20% of the reference run.

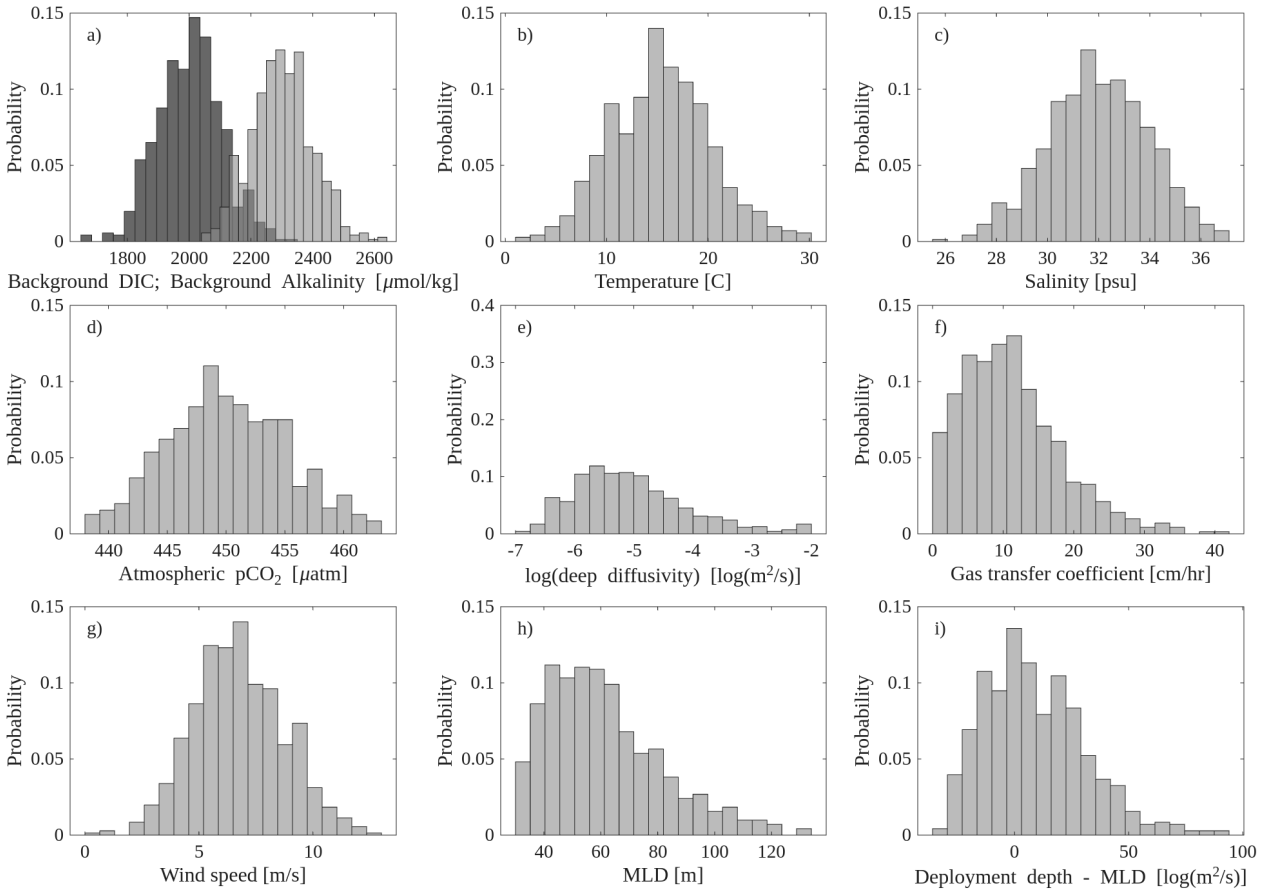


Figure 6. Distributions for input parameters used in Monte Carlo simulations. Uncertainties in atmospheric partial pressure of CO_2 (pCO_2), temperature (Temp), salinity (Salt) and initial concentrations of total alkalinity (TA) and dissolved inorganic carbon (DIC) are assumed to be normally distributed with mean and standard deviations given by Table 1. Uncertainties in mixed layer depth (MLD), the logarithm of diffusivity and the deployment depth with respect to the mixed layer depth are described by a Pearson Type 1 distribution.

Parameter	Mean	St. Dev.	Skewness	Kurtosis
Initial mixed layer TA (A_{ML}) [μmol/kg]	2300	100	0	0
Initial mixed layer DIC (C_{ML}) [μmol/kg]	2000	100	0	0
Initial deep TA (A_{Deep}) [μmol/kg]	2300	100	0	0
Initial deep DIC (C_{Deep}) [μmol/kg]	2000	100	0	0
Mixed layer temperature (T_{ML}) [C]	15	5	0	0
Mixed layer salinity (S_{ML}) [psu]	32	2	0	0
Atmospheric pCO_2 (pCO_2^{atm}) [μatm]	450	5	0	0
Deep diffusivity ($\log_{10}\kappa_{deep}$) [$\log_{10}(m^2s^{-1})$]	-5	1	0.9	4
10m Wind speed (u_{wind}) [m/s]	6.4	2	0	0
Gas Transfer Coefficient (k_g) [cm/hr]	W14 $f(u_{wind},T,S)$	4	0	0
Mixed Layer Depth (H_{ML}) [m]	60	20	1	4
Deployment Depth (z_{depl}) [m]	1.1*H_{ML}	20	1	4

Table 1. *Distribution characteristics for model state estimates of variables in baseline simulations in 1D model. Intervention simulations are identical to baseline simulations with an additional TA of* 2.048×10^6 *mol. Most parameters follow a Normal distribution, with specified mean and standard deviations. Non-symmetric distributions are defined as Pearson Type 1 Distributions with mean, standard deviation, kurtosis and skewness. "Deployment depth" is the maximum depth of the alkalinity addition, and its distribution is set such that around 50% of initial alkalinity additions have maximum depths just below the mixed layer. "Reference" simulations use mean values, while "Sensitivity" simulations use variables plus or minus one standard deviation, except for deployment depth sensitivities which set* z_{depl} *to 20 or 40m below the mixed layer . "Monte Carlo" simulations draw variables at random from the distributions specified by this table.*

A Vertical structure of initial profiles of DIC, alkalinity and diffusivity

Initial DIC profiles are always uniform in depth. Initial TA profiles for baseline simulations are uniform in depth, while the intervention has a fixed additional mass of TA distributed either over the mixed layer (for deployment depths shallower than the mixed layer depth), or over a layer 60 m deep for deployments at a depth of z_{depl} (Fig 7a). Diffusivity profiles are defined:

$$\log\kappa = \frac{\Delta\log\kappa}{2}(\tanh((z-H_{ML})/4)+1)+\log\kappa_{pyc} \tag{11}$$

where $\Delta\log\kappa = \log\kappa_{upper} - \log\kappa_{deep}$. $\kappa_{upper} = 10^2$ m^2/s and is fixed for all runs, while the deep value varies according to the parameters defined in Table 1. An example profile for the Reference simulation is provided in Figure 7b.

B Uncertainties in the gas transfer coefficient

Using data from eight field experiments made available by [40], the standard deviation in the gas transfer coefficient for a given wind speed across all experiments is calculated in Figure 8. Variability in the gas transfer coefficient between each experiment arises from regional and seasonal effects, and this variability is more pronounced at higher wind speeds.

C Derivation of the timescale for loss of modified waters from the mixed layer

By averaging eqs 5 over the mixed layer and a deep layer, one can form a two-box model that evolves the averaged properties of TA and DIC in each box. In the case of alkalinity, the resulting governing equations are:

$$\frac{\partial\overline{A}_{ML}}{\partial t} = -\frac{1}{H_{ML}}\kappa_{pyc}\frac{\overline{A}_{ML}-\overline{A}_{Deep}}{h_p} \tag{12}$$

$$\frac{\partial\overline{A}_{Deep}}{\partial t} = \frac{1}{(D-H_{ML})}\kappa_{pyc}\frac{\overline{A}_{ML}-\overline{A}_{Deep}}{h_p}. \tag{13}$$

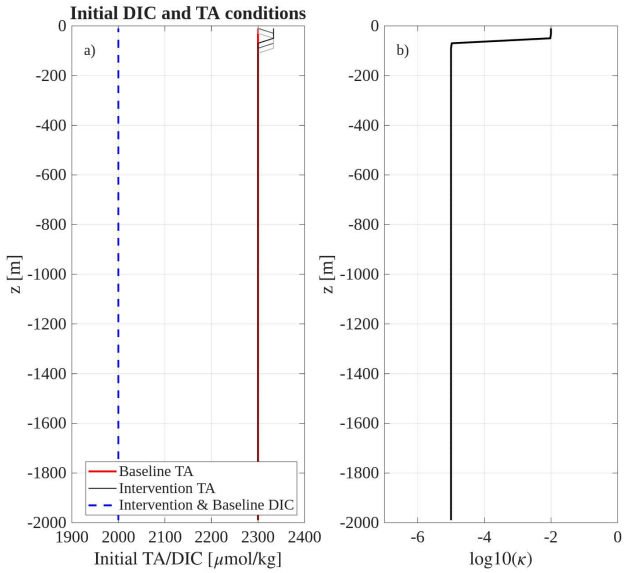


Figure 7. a) Example initial conditions for DIC (blue dashed) and TA (red: baseline; blacks/greys: perturbation). Black and grey lines show initial TA in intervention simulation for TA deployed with the base 20m and 40m below the mixed layer. b) Diffusivity profile for Reference simulations.

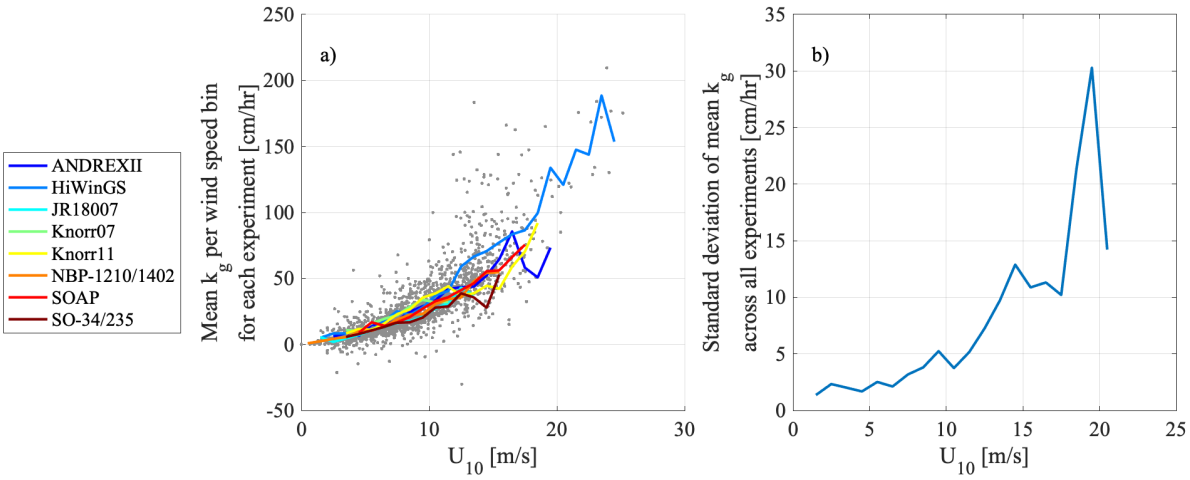


Figure 8. a) Hourly estimates (grey dots) of the gas transfer experiment are averaged for each experiment. b) The standard deviation in estimates for a given wind speed across all experiments indicate the uncertainties.

where overlines indicate box average properties, κ_{pyc} is the diffusivity evaluated at the interface between the mixed layer and deep boxes (i.e. in the pycnocline), h_p is the thickness of the pycnocline (set to 150 m) and D is the ocean depth.

Subtracting the equation for deep alkalinity from mixed layer alkalinity, we define a new variable, $\gamma = \overline{A}_{ML} - \overline{A}_{Deep}$ to form the differential equation

$$\frac{\partial \gamma}{\partial t} = -\gamma \left(\frac{D\kappa_{pyc}}{H_{ML} h_p (D - H_{ML})} \right). \tag{14}$$

Solutions to this equation are exponential with a timescale $\tau_{mix} = \frac{H_{ML} h_p (D - H_{ML})}{D\kappa_{pyc}}$.

Acknowledgements

The author thanks Alex Hay and Clark Richards for providing comments on a draft of this manuscript, and Erik Johnson and Josiane Ostiguy for stimulating conversations on the topic.

Funding

Funding from the Canada Research Chairs Program is gratefully acknowledged.

Open Research Section

All codes required to run the simulations described in this manuscript are available in a private Github repository, which will be made public upon the publication of this work. A tagged release of the repository is available for the reviewers here.

References

1. National Academies of Sciences. *Climate Intervention: Carbon Dioxide Removal and Reliable Sequestration* (National Academies Press, Washington, D.C., 2015).

2. National Academies of Sciences. *Negative Emissions Technologies and Reliable Sequestration: A Research Agenda* (National Academies Press, Washington, D.C., 2019).

3. National Academies of Sciences. *A Research Strategy for Ocean-based Carbon Dioxide Removal and Sequestration* (National Academies Press, Washington, D.C., 2022).

4. Digdaya, I. A. *et al.* A direct coupled electrochemical system for capture and conversion of CO_2 from oceanwater. *Nat Commun* **11**, 4412, DOI: 10.1038/s41467-020-18232-y (2020).

5. Schulz, K. G., Bach, L. T. & Dickson, A. G. Seawater carbonate chemistry considerations for ocean alkalinity enhancement research: Theory, measurements, and calculations. *State Planet* **2-oae2023**, 1–14, DOI: 10.5194/sp-2-oae2023-2-2023 (2023).

6. He, J. & Tyka, M. D. Limits and CO_2 equilibration of near-coast alkalinity enhancement. *Biogeosciences* 27–43, DOI: 10.5194/bg-20-27-2023 (2023).

7. Zhou, M. *et al.* Mapping the global variation in the efficiency of ocean alkalinity enhancement for carbon dioxide removal. *Nat. Clim. Chang.* **15**, 59–65, DOI: 10.1038/s41558-024-02179-9 (2025).

8. Ho, D. T. *et al.* Monitoring, reporting, and verification for ocean alkalinity enhancement. *State Planet* **2-oae2023**, 1–12, DOI: 10.5194/sp-2-oae2023-12-2023 (2023).

9. Fennel, K. *et al.* Modeling considerations for research on ocean alkalinity enhancement (OAE). *State Planet Discuss.* **2023**, 1–47 (2023).

10. Yankovsky, E. *et al.* Impulse response functions as a framework for quantifying ocean-based carbon dioxide removal. *Biogeosciences* **22**, 5723–5739 (2025).

11. Xie, Y., Spence, P., Corney, S., Tyka, M. D. & Bach, L. T. Effect of model resolution on air-sea CO_2 equilibration timescales. *Glob. Biogeochem. Cycles* **39**, e2024GB008482 (2025).

12. Griffies, S. M. *et al.* Developments in ocean climate modelling. *Ocean. Model.* **2**, 123–192 (2000).

13. Griffa, A., Piterbarg, L. I. & Özgökmen, T. Predictability of Lagrangian particle trajectories: effects of smoothing of the underlying Eulerian flow. *J. Mar. Res.* **62** (2004).

14. Foteinis, S., Campbell, J. S. & Renforth, P. Life Cycle Assessment of Coastal Enhanced Weathering for Carbon Dioxide Removal from Air. *Environ. Sci. Technol.* **57**, 6169–6178, DOI: 10.1021/acs.est.2c08633 (2023).

15. Waterhouse, A. F. *et al.* Global Patterns of Diapycnal Mixing from Measurements of the Turbulent Dissipation Rate. *J. Phys. Oceanogr.* **44**, 1854–1872, DOI: 10.1175/JPO-D-13-0104.1 (2014).

16. Trossman, D. S. *et al.* Tracer and observationally derived constraints on diapycnal diffusivities in an ocean state estimate. *Ocean. Sci.* **18**, 729–759, DOI: 10.5194/os-18-729-2022 (2022).

17. Sarmiento, J. L. & Gruber, N. *Ocean Biogeochemical Dynamics* (Princeton university press, 2013).

18. Jones, D. C., Ito, T., Takano, Y. & Hsu, W.-C. Spatial and seasonal variability of the air-sea equilibration timescale of carbon dioxide. *Glob. Biogeochem. Cycles* **28**, 1163–1178, DOI: 10.1002/2014GB004813 (2014).

19. Foteinis, S., Andresen, J., Campo, F., Caserini, S. & Renforth, P. Life cycle assessment of ocean liming for carbon dioxide removal from the atmosphere. *J. Clean. Prod.* **370**, 133309, DOI: 10.1016/j.jclepro.2022.133309 (2022).

20. Berglund, S., Döös, K., Groeskamp, S. & McDougall, T. J. The downward spiralling nature of the North Atlantic Subtropical Gyre. *Nat. communications* **13**, 2000 (2022).

21. MacKinnon, J. A. *et al.* Climate Process Team on Internal Wave–Driven Ocean Mixing. *Bull. Am. Meteorol. Soc.* **98**, 2429–2454, DOI: 10.1175/BAMS-D-16-0030.1 (2017).

22. Melet, A., Hallberg, R., Legg, S. & Polzin, K. Sensitivity of the Ocean State to the Vertical Distribution of Internal-Tide-Driven Mixing. *J. Phys. Oceanogr.* **43**, 602–615, DOI: 10.1175/JPO-D-12-055.1 (2013).

23. Melet, A., Hallberg, R., Adcroft, A., Nikurashin, M. & Legg, S. Energy Flux into Internal Lee Waves: Sensitivity to Future Climate Changes Using Linear Theory and a Climate Model. *J. Clim.* **28**, 2365–2384, DOI: 10.1175/JCLI-D-14-00432.1 (2015).

24. Ehlert, D., Zickfield, K., Eby, M. & Gillett, N. The Sensitivity of the Proportionality between Temperature Change and Cumulative CO_2 Emissions to Ocean Mixing. *J. Clim.* 2921 – 2935 (2017).

25. Lamont, J. C. & Scott, D. S. An eddy cell model of mass transfer into the surface of a turbulent liquid. *AIChE J.* **16**, 513–519, DOI: 10.1002/aic.690160403 (1970).

26. Deike, L. & Melville, W. K. Gas Transfer by Breaking Waves. *Geophys. Res. Lett.* **45**, DOI: 10.1029/2018GL078758 (2018).

27. Zhou, X., Reichl, B. G., Romero, L. & Deike, L. A Sea State Dependent Gas Transfer Velocity for CO_2 Unifying Theory, Model, and Field Data. *Earth Space Sci.* **10**, e2023EA003237, DOI: 10.1029/2023EA003237 (2023).

28. Fu, W. *et al.* Evaluation of Ocean Biogeochemistry and Carbon Cycling in CMIP Earth System Models With the International Ocean Model Benchmarking (IOMB) Software System. *J. Geophys. Res. Ocean.* **127**, e2022JC018965, DOI: https://doi.org/10.1029/2022JC018965 (2022). E2022JC018965 2022JC018965, https://agupubs.onlinelibrary.wiley.com/doi/pdf/10.1029/2022JC018965.

29. Planchat, A. *et al.* The representation of alkalinity and the carbonate pump from CMIP5 to CMIP6 Earth system models and implications for the carbon cycle. *Biogeosciences* **20**, 1195–1257, DOI: 10.5194/bg-20-1195-2023 (2023).

30. Hinrichs, C., Köhler, P., Völker, C. & Hauck, J. Alkalinity biases in CMIP6 Earth system models and implications for simulated CO_2 drawdown via artificial alkalinity enhancement. *Biogeosciences* **20**, 3717–3735, DOI: 10.5194/bg-20-3717-2023 (2023).

31. Weiss, R. Carbon dioxide in water and seawater: The solubility of a non-ideal gas. *Mar. Chem.* **2**, 203–215, DOI: 10.1016/0304-4203(74)90015-2 (1974).

32. Ho, D. T. *et al.* Measurements of air-sea gas exchange at high wind speeds in the Southern Ocean: Implications for global parameterizations. *Geophys. Res. Lett.* **33**, 2006GL026817, DOI: 10.1029/2006GL026817 (2006).

33. Wanninkhof, R. Relationship between wind speed and gas exchange over the ocean revisited: Gas exchange and wind speed over the ocean. *Limnol. Ocean. Methods* **12**, 351–362, DOI: 10.4319/lom.2014.12.351 (2014).

34. Sharp, J. D. *et al.* CO2SYSv3 for MATLAB. Zenodo, DOI: 10.5281/zenodo.7552554 (2023).

35. Large, W. G., McWilliams, J. C. & Doney, S. C. Oceanic vertical mixing: A review and a model with a nonlocal boundary layer parameterization. *Rev. Geophys.* **32**, 363, DOI: 10.1029/94RG01872 (1994).

36. St. Laurent, L. C., Simmons, H. L. & Jayne, S. R. Estimating tidally driven mixing in the deep ocean. *Geophys. Res. Lett.* **29**, 21–1–21–4, DOI: 10.1029/2002GL015633 (2002).

404 **37.** Ledwell, J. R., Watson, A. J. & Law, C. S. Evidence for slow mixing across the pycnocline from an open-ocean
405 tracer-release experiment. *Nature* **364**, 701–703 (1993).

406 **38.** Ledwell, J. R., St. Laurent, L. C., Girton, J. B. & Toole, J. M. Diapycnal Mixing in the Antarctic Circumpolar Current. *J.*
407 *Phys. Oceanogr.* **41**, 241–246, DOI: 10.1175/2010JPO4557.1 (2011).

408 **39.** Cael, B. B. & Mashayek, A. Log-Skew-Normality of Ocean Turbulence. *Phys. Rev. Lett.* **126**, 224502, DOI: 10.1103/
409 PhysRevLett.126.224502 (2021).

410 **40.** Yang, M. *et al.* Global Synthesis of Air-Sea CO_2 Transfer Velocity Estimates From Ship-Based Eddy Covariance
411 Measurements. *Front. Mar. Sci.* **9**, 826421, DOI: 10.3389/fmars.2022.826421 (2022).